FISEVIER

Contents lists available at ScienceDirect

### Journal of Colloid and Interface Science

journal homepage: www.elsevier.com/locate/jcis



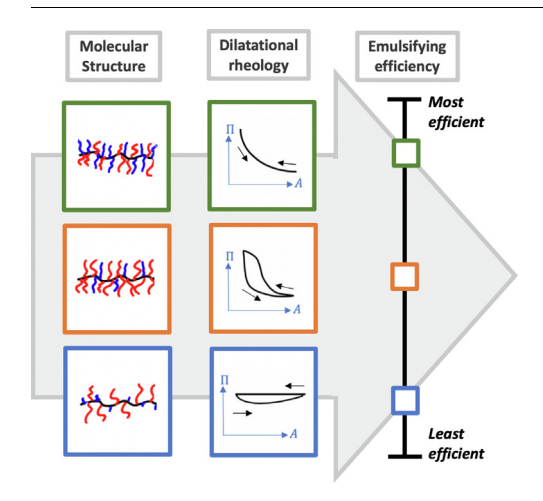
## Interfacial dilatational rheology as a bridge to connect amphiphilic heterografted bottlebrush copolymer architecture to emulsifying efficiency



Tsung-Lin Hsieh<sup>a</sup>, Michael R. Martinez<sup>b</sup>, Stephen Garoff<sup>c</sup>, Krzysztof Matyjaszewski<sup>b</sup>, Robert D. Tilton<sup>a,d,\*</sup>

- <sup>a</sup> Department of Chemical Engineering, Center for Complex Fluids Engineering, Carnegie Mellon University, Pittsburgh, PA 15213 USA
- <sup>b</sup> Department of Chemistry, Center for Complex Fluids Engineering, Carnegie Mellon University, Pittsburgh, PA 15213 USA
- <sup>c</sup> Department of Physics, Center for Complex Fluids Engineering, Carnegie Mellon University, Pittsburgh, PA 15213 USA
- d Department of Biomedical Engineering, Center for Complex Fluids Engineering, Carnegie Mellon University, Pittsburgh, PA 15213, USA

#### G R A P H I C A L A B S T R A C T



#### ARTICLE INFO

Article history: Received 7 April 2020 Revised 12 July 2020 Accepted 13 July 2020 Available online 17 July 2020

Keywords:
Dilatational modulus
Bottlebrush copolymer
Fluid interface
Interfacial tension
Emulsifying efficiency

#### $A\ B\ S\ T\ R\ A\ C\ T$

*Hypothesis*: Molecular architecture and composition of amphiphilic bottlebrush copolymers will dictate the dominant interfacial relaxation modes and the corresponding dilatational rheology for adsorbed layers at oil/water interfaces in a way that will correlate with the emulsifying efficiency of different bottlebrush copolymers.

Experiments: Amphiphilic, xylene-soluble poly(ethylene oxide)-poly(*n*-butyl acrylate) (PEO-PBA) heterografted bottlebrush copolymers with controlled differences in backbone length, hydrophilicity and arm length were synthesized by atom transfer radical polymerization. Dilatational rheology of adsorbed layers at the xylene/water interface was probed via pendant drop tensiometry by measuring the interfacial stress response to either large-amplitude strain cycling or small-amplitude strain oscillation. The rheological response was recorded as a function of interfacial pressure for adsorbed layers under different compression states. Emulsifying efficiency was determined as the lowest copolymer concentration that yielded water-in-xylene emulsions with at least one-month stability against coalescence.

<sup>\*</sup> Corresponding author at: Department of Chemical Engineering, Center for Complex Fluids Engineering, Carnegie Mellon University, Pittsburgh, PA 15213, USA. E-mail address: tilton@cmu.edu (R.D. Tilton).

Findings: The more hydrophilic copolymers with longer PEO arms exhibited non-hysteretic stress-strain response curves in large-amplitude strain cycling and a tendency for the modulus to increase with increasing interfacial pressure. These were more efficient emulsifiers than less hydrophilic copolymers that exhibited hysteretic interfacial rheology. Mere existence of significant moduli did not correlate with high emulsifying efficiency, while an increase in modulus with increasing interfacial pressure did so.

© 2020 The Author(s). Published by Elsevier Inc. This is an open access article under the CC BY-NC-ND license (http://creativecommons.org/licenses/by-nc-nd/4.0/).

#### 1. Introduction

Interfacial rheology probes the stress-strain relations of interfacial layers at fluid interfaces and typically is investigated to determine how the composition of an adsorbed layer of surfactants [1], polymers [2,3], proteins [4,5], nanoparticles [6,7], or other surfaceactive materials controls the dynamic mechanical properties of the interface. Stress-strain relations are commonly measured for one of two deformation modes: an interfacial shape change at constant area (shearing) or an interfacial area change at constant shape (dilatation). Understanding the interfacial rheological response to interfacial deformation, especially dilatation, under varying strain rate and amplitude conditions is often motivated by the relevance of dynamic interfacial mechanical properties to the production, dynamics and stability of emulsions [8–10], foams [11,12] or other formulated multi-phase systems.

The dilatational modulus of an adsorbed layer represents the resistance to interfacial area expansion or compression. For an interfacial system that fully equilibrates on the perturbation timescale, the Gibbs dilatational elasticity (E) is defined as the change of equilibrium interfacial pressure ( $\Pi_e$ ) in response to a relative change of interfacial concentration ( $\Gamma$ ). This would be caused by an imposed perturbation to the interfacial area (A) at constant number of adsorbed species:

$$E = \left(\frac{\partial \Pi_e}{\partial ln\Gamma}\right)_{N,T} = -\left(\frac{\partial \Pi_e}{\partial lnA}\right)_{N,T} \tag{1}$$

The Gibbs dilatational elasticity is an equilibrium thermodynamic state property of a closed interfacial system, excluding effects of any dynamic relaxation processes that may occur at the interface. In general, we can define the dynamic dilatational modulus  $(E_d)$  from the possibly non-equilibrium interfacial pressurearea  $(\Pi - A)$  response curve:

$$E_d = -\left(\frac{\partial \Pi}{\partial lnA}\right)_T \tag{2}$$

A common experiment is to impose a small-strain sinusoidal area perturbation at some angular frequency  $\omega$ . Generally, the modulus in this case is a complex number if the interface undergoes some relaxation during perturbation:

$$E^{*}(\omega) = \frac{F_{\omega}\{-\Delta\Pi\}}{F_{\omega}\{\Delta\ln A\}} = E'(\omega) + iE''(\omega)$$
(3)

where  $F_{\omega}\{x\}$  is the Fourier transform evaluated at the fundamental frequency of the imposed perturbation and the complex dilatational modulus  $(E^*)$  consists of a storage modulus (E') and a loss modulus (E''). Interpreting the frequency dependence of this complex modulus based on relevant relaxation modes is a goal of dilatational rheology. Since Lucassen and van den Tempel developed their diffusion-limited model (LVDT model) for the complex dilatational modulus of a soluble surfactant system [13], a series of models based on more complicated relaxations (e.g. micellization [14], adsorption with energetic barriers [15], binary surfactant transport [16], or linear polymer reconfiguration [17]) has also been developed.

Progress connecting surfactant molecular structure and dilatational rheological behavior has been made in recent years. Noskov and coworkers studied in detail how the protein structure may affect the dilatational behavior of adsorbed protein layers [18-20]. Not only did they compare proteins with different structures, but they also studied the influence of denaturants on the protein structure and its effect on dilatational rheology. They found that while the rheological behaviors of globular proteins tend to resemble the behaviors of nanoparticles at the interface, where the dilatational modulus increases monotonically with increasing adsorption, non-globular proteins behave more like nonionic amphiphilic linear polymers, where the variation is nonmonotonic. Huang and coworkers compared the adsorption and dilatational behaviors of a series of linear poly(ethylene oxide) (PEO) polymers and a multi-arm PEO star polymer. The compact multi-arm PEO star polymer exhibited a large dilatational modulus, whereas the highly flexible linear PEO chains produced no detectible modulus [3]. In contrast, Alvarez and coworkers showed that adsorbed polyelectrolytes could exhibit similar dilatational moduli as polyelectrolyte-grafted nanoparticles [21]. This can be attributed to the stiffness of the polyelectrolytes.

A number of studies have established a connection between dilatational rheology of emulsifier-laden interfaces and the stability of emulsions produced with different types of emulsifiers [8-10,22-24]. Emulsifiers that produce large dilatational moduli tend to be effective emulsifiers, with Ostwald ripening or coalescence mechanisms tending to correlate with moduli measured in different frequency ranges. That literature focuses on the effectiveness of the emulsifiers rather than their emulsifying efficiency. The former refers to the ability to stabilize emulsions against coalescence over long time periods, while the latter refers to the ability to do so at low emulsifier concentrations. Consideration of emulsifying efficiency not only must consider factors favoring emulsion stability under quiescent conditions but also factors involved in emulsion formation during high shear homogenization processes. Strains and strain rates sampled during emulsification are much different from those during quiescent conditions under which stability is assessed. Emulsifying effectiveness and efficiency are not equivalent concepts. There are systems of emulsifiers that differ significantly in their emulsifying efficiency but not in effectiveness [25]. Accordingly, one may anticipate that interfacial rheological factors favoring high efficiency may not be the same as those favoring long-term stability.

In recent years, a class of polymer structures with a shared architectural characteristic of having multiple arms tethered to a core, including multi-arm star polymers, polymer brush-grafted nanoparticles, or bottlebrush polymers with multiple arms emanating from a linear polymer backbone, have been reported to be extremely efficient emulsifiers [3,25–30]. These can stabilize emulsions for months to years, using bulk polymer concentrations that are three to four orders of magnitude lower than normally needed for conventional emulsifiers to achieve similar long-term stabilization. In the present work, we investigate the interfacial dilatational rheology of a series of amphiphilic, heterografted bottlebrush copolymers with PEO and poly(*n*-butyl acrylate) (PBA) sidechain "arms". These are adsorbed from solutions in xylene to the

xylene/water interface. The series of copolymers investigated here provides systematic variations in the ratio of hydrophilic PEO and hydrophobic PBA arms, the arm degree of polymerization, and the backbone degree of polymerization. We elucidate how distinguishing dilatational rheological characteristics connect the emulsifying efficiency of a bottlebrush copolymer with its architectural features.

#### 2. Materials and methods

# 2.1. Synthesis and characterization of PEO-PBA heterografted bottlebrush copolymers

A copolymer nomenclature is defined in Section 3.1 to represent each material according to the relative amounts of hydrophilic PEO and hydrophobic PBA arms, the backbone degree of polymerization, and the arm degree of polymerization. The synthetic procedure used to prepare H16-B001, H17-B365, H06-B315, and H07-B270-SA was previously reported [30]. H20-B075 and H18-B150 were prepared using a similar synthetic procedure, and all synthetic details are provided in Section 1 of Supporting Information. The heterografted PEO-PBA bottlebrush copolymers were prepared in three steps.

First, atom transfer radical polymerization (ATRP) of poly(ethylene oxide) monomethyl ether methacrylate (OEOMA) with a pro-(2-trimethylsiloxy)ethyl methacrylate (HEMA-TMS) comonomer was performed. The P(PEOMA-stat-HEMA-TMS) copolymer was then deprotected and functionalized with  $\alpha$ bromoisobutyrate initiators by base catalyzed transesterification a statistical poly(2-bromoisobutyryloxyethyl methacrylate)-stat-poly(ethylene glycol) methyl ether methacrylate (P(BiBEM-stat-PEOMA)) copolymer. P(BiBEM-stat-PEOMA) was used as a multifunctional macroinitiator for grafting-from ATRP of BA to produce poly((2-bromoisobutyryloxyethyl methacrylate-graft-poly(n-butyl acrylate))-stat-poly(ethylene glycol) methyl ether methacrylate (P[BiBEM-g-PBA]-stat-PEOMA). P [BiBEM-g-PBA]-stat-PEOMA is a bottlebrush copolymer with a statistical distribution of monomers with PBA arms or PEO arms. Copolymers of different backbone lengths, different relative amounts of PEO and PBA content, and different arm lengths were prepared. The apparent molecular weight  $(M_n)$  and dispersity (D)of each polymer were measured by gel permeation chromatography (GPC). The GPC utilized tetrahydrofuran as the eluent at a flow rate of 1 mL min<sup>-1</sup> and temperature of 35 °C with a Waters 515 pump and Waters 2414 refractive index detector. The GPC was equipped with PSS columns (SDV 10<sup>5</sup>, 10<sup>3</sup>, 500 Å) calibrated against linear poly(methyl methacrylate) (PMMA) standards. The monomer conversion of all polymerizations and compositions of purified samples were measured via proton nuclear magnetic resonance (<sup>1</sup>H NMR) spectroscopy using a Bruker Advance 300 or 500 MHz NMR spectrometer with deuterated chloroform (CDCl<sub>3</sub>) as the solvent.

#### 2.2. Pendant drop tensiometry

The interfacial tension at the xylene/water interface, which we denote generally as interfacial stress ( $\sigma$ ) to emphasize its possible non-equilibrium character, was measured by pendant drop tensiometry (Biolin Scientific Optical Tensiometer). All water was first de-ionized by reverse osmosis and further ultra-purified to 18 M $\Omega$ cm resistivity by a Barnstead Nanopure Diamond system. Xylene (mixture of m, p, and o-isomers with purity  $\geq$ 98.5%) was from Fisher Chemical and used as received. Further xylene purification by passage through a column of basic-activated alumina (Beantown Chemical) did not change its interfacial tension against

water, indicating the as-received xylene was sufficiently free of surface-active impurities [3]. All copolymers were water insoluble and were dissolved in xylene for all measurements. All experiments were conducted at room temperature  $21.4 \pm 0.3$  °C.

A drop of water, typically 20–30 μL in volume, was generated at the tip of a needle immersed in the polymer solution and imaged as a function of time as copolymers adsorbed from the xylene phase to the xylene/water interface. With the use of One Attension software (Biolin Scientific Optical Tensiometer), the drop shape was digitized and used to calculate the interfacial area as well as the interfacial stress by fitting to the Young-Laplace equation. All drop shapes were verified not to significantly deviate from the Young-Laplace shapes (See Supporting Information Section 2). The dynamic interfacial stress was monitored during adsorption after initially generating the drop for two different bulk polymer concentrations (0.005 wt% and 0.1 wt% in xylene). The interface state at 1000 s was chosen to be the "initial state" of the adsorbed layer for further rheological measurements. This time was selected because in all cases examined, the rate of change of the decreasing interfacial stress was consistently less than 0.2 mNm<sup>-1</sup>min<sup>-1</sup> after 1000 s of adsorption.

#### 2.3. Dilatational rheology

The dilatational modulus of an adsorbed layer represents the resistance to changes in the interfacial area. It is usually determined from the variation of the interfacial pressure ( $\Pi=\gamma_o-\sigma$ , where  $\gamma_o$  is the equilibrium interfacial tension of the clean interface without adsorption) during area perturbation. In this work, the dynamic dilatational modulus was measured at varying interfacial pressures in two types of experiments: (1) Large-amplitude strain cycling experiments and (2) small-amplitude strain oscillation experiments. Both types of experiments perturbed the interfacial area over several cycles, but with different wave forms and amplitudes of the forcing function. Results from these two forms of interfacial rheology experiments were compared.

#### 2.3.1. Large-amplitude strain cycling experiments

Starting from the initial state achieved after 1000 s of adsorption, three large-amplitude strain compression and expansion cycles were imposed with an area strain  $\Delta A/A_0$  ranging from approximately 40-80%. The area perturbation approximated a triangle wave with a nearly constant rate of area change. The instrument's control system fixes a constant rate of volume change: the rates used here corresponded to a nearly constant area dilatation rate of  $0.026 \pm 0.001 \text{ mm}^2\text{s}^{-1}$ , and area strain rates  $\frac{d\ln A}{dt}$  ranged from ~0.001-0.01 s<sup>-1</sup> from the beginning to the end of each large amplitude compression stage for the drop sizes used here. The maximum extent of compression would ultimately be limited by the point at which the critical Bond number would be reached and the drop would fall from the needle. This was determined separately so that cycling experiments never reached the critical Bond number. The interfacial pressure during the compression and expansion cycles was recorded and the "compression modulus" was calculated as a function of  $\Pi$  using Eq. [2], similar to previous publications [3,31].

### 2.3.2. Small-amplitude strain oscillation experiments

At the initial state achieved after 1000 s of adsorption, the interfacial area was subjected to small-amplitude oscillatory perturbations by sinusoidally oscillating the drop volume with an area strain amplitude ~1%. Oscillation frequencies, f, were varied from 0.05 to 1 Hz. Once the stress and the strain were verified, by Fourier transform, to be sinusoidal with negligible higher harmonics, the complex dilatational modulus ( $E^* = E^{'} + iE^{''}$ ) was obtained by

fitting the measured  $\Pi(t)$  to the experimentally imposed strain and strain rate according to

$$-\Delta\Pi(t) = E'\varepsilon(t) + \frac{E''}{\omega} \frac{d\varepsilon(t)}{dt}$$
 [4]

where  $\varepsilon(t)=rac{A(t)-A_0}{A_0}$  is the strain,  $rac{darepsilon(t)}{dt}$  is the strain rate and  $\omega=2\pi f$  is the angular frequency of the perturbation.

After determining the complex modulus at the initial adsorbed layer state, the drop was stepwise compressed in interfacial pressure increments of approximately 2 to 5 mN/m to reach a new interfacial pressure, at which point a new series of oscillatory measurements spanning the 0.05-1 Hz frequency range was conducted. The wait time from the end of compression to the onset of the subsequent oscillation was about 1 min, during which no significant relaxation in interfacial stress was observed. In addition, no significant drift of interfacial stress was observed during the oscillation measurements. For the drop volumes considered here, the maximum area dilatation rate in these experiments ranged from approximately 0.094 to 1.9 mm<sup>2</sup>s<sup>-1</sup> (varying with frequency), and the corresponding strain rate ranged from approximately 0.0036 to 0.1  $s^{-1}$  (varying with  $A_0$  and frequency). Although the drop volume, rather than drop area, was sinusoidally oscillated via the instrument's control system, Fourier analysis indicated no significant deviation from sinusoidal area oscillation for the perturbations imposed here.

#### 2.4. Emulsification test

Emulsions were generated using each of the bottlebrush copolymers in order to discern whether there were correlations among the bottlebrush copolymer structures, their dominant dilatational rheology relaxation modes, and their emulsifying efficiencies. Water/xylene emulsions were prepared by vortex mixing (Fisher Scientific Analogue Vortex Mixer, 3000 rpm) for 30 s with equal masses of water and polymer solutions in xylene, for various copolymer concentrations (expressed as wt% on the basis of polymer mass per total mass of xylene plus water). Drop tests were performed to determine that emulsions were water-in-xylene (W/O): a drop of a W/O emulsion disperses readily when placed atop a bulk sample of the oil but not when placed on water. Emulsifying efficiency was reported as the lowest copolymer concentration at which a stable emulsion was formed without the appearance of a neat water phase for at least one month.

#### 3. Results and discussion

#### 3.1. Polymer characterization

Characteristics of the bottlebrush copolymers are summarized in Table 1. The copolymers are illustrated schematically in Fig. 1

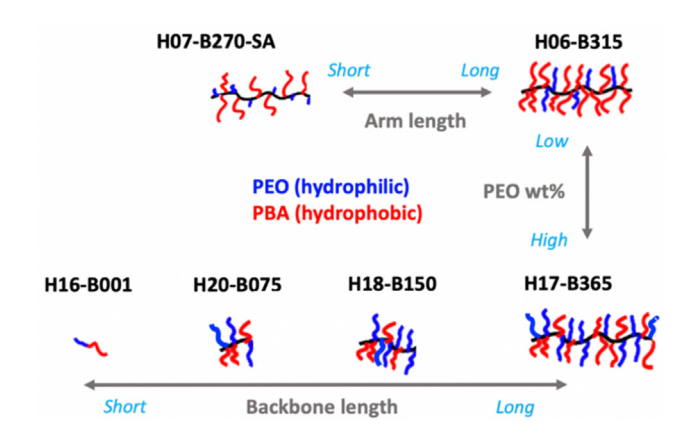


**Fig. 1.** Schematic representations of bottlebrush copolymers to demonstrate the variation in arm length, PEO content and backbone length.

and identified by the nomenclature H (hydrophilic PEO wt%)-B (backbone degree of polymerization). Most of the polymers have PEO arms with degree of polymerization (DP) 23 and PBA arms with DP 30. One sample was prepared with PEO arms of 7 DP and PBA arms of 15 DP. The nomenclature for this "short-arm" sample includes a suffix "SA". Thus, H07-B270-SA has 7 wt% PEO, a backbone DP of 270 and short side-chains. The full series of copolymers allowed a comparison of similar compositions with differing arm length, similar backbone lengths with varying hydrophilicity (PEO wt%), similar hydrophilicity with varying backbone length, as well as a linear diblock copolymer that can be loosely considered as having "backbone" DP of one for the purposes of comparison. For more details about the characterization, readers are referred to Supporting Information Section 1 as well as a prior publication by Xie and coworkers [30].

#### 3.2. Dynamic interfacial stress

Fig. 2 reports the interfacial stress evolution in the first 1000 s after creating the water drop in the copolymer solution at 0.005 or 0.1 wt%. The measured interfacial tension of the clean xylenewater interface was  $37.4 \pm 0.1$  mN/m. This is consistent with previously reported values [3,30].

All copolymers decreased the interfacial stress of the xylene/ water interface. Focusing on the long-time behavior, for copolymers with similar PEO content (H16-B001, H20-B075, H18-B150 and H17-B365), the copolymer with the longest backbone (H17-B365) decreased interfacial tension the least, but the long-time adsorption data appeared in two clusters. Most of the high-PEO content copolymers appeared in the large interfacial stress reduction cluster while H17-B365 fell in the low interfacial stress reduction cluster.

**Table 1**Characteristics of bottlebrush copolymers

Copolymers	Wt.% PEO	Mol. % PEO <sup>a</sup>	Molecular Parameters <sup>b</sup>			$M_{n,theo}^{b}$ (10 <sup>6</sup> g/mol)	$\mathrm{M_{n,GPC}}^{\mathrm{c}}$ (10 <sup>6</sup> g/mol)	Đ <sup>€</sup>
			DP <sub>PEOMA</sub>	$DP_{BiBEM}$	$DP_{PnBA}$			
H16-B001	16	50	=	=	41	0.00638	0.00933	1.22
H20-B075	20	48	36	39	26	0.175	0.079	1.06
H18-B150	18	47	71	79	27	0.365	0.173	1.24
H17-B365	17	46	167	198	29	0.960	0.138	1.22
H06-B315	6	23	73	242	32	1.13	0.232	1.13
H07-B270-SA	7	37	99	171	15	0.407	0.207	1.30

<sup>&</sup>lt;sup>a</sup> Calculated based on <sup>1</sup>H NMR of P(BiBEM) (m, broad, OCO – CH2–, 4.29–4.50 ppm) to P(PEOMA) (m, broad, O – CH2 – CH2–, 3.59–3.71 ppm).

 $<sup>^{\</sup>rm b}\,$  Calculated based on conversion of monomer determined by  $^{\rm 1}{\rm H}$  NMR.

<sup>&</sup>lt;sup>c</sup> Molecular weight and dispersity measured by THF GPC calibrated using linear PMMA standards. The difference between  $M_{n,theo}$  and  $M_{n,GPC}$  serves as a measure of the structural compactness of multi-branched polymers [32].

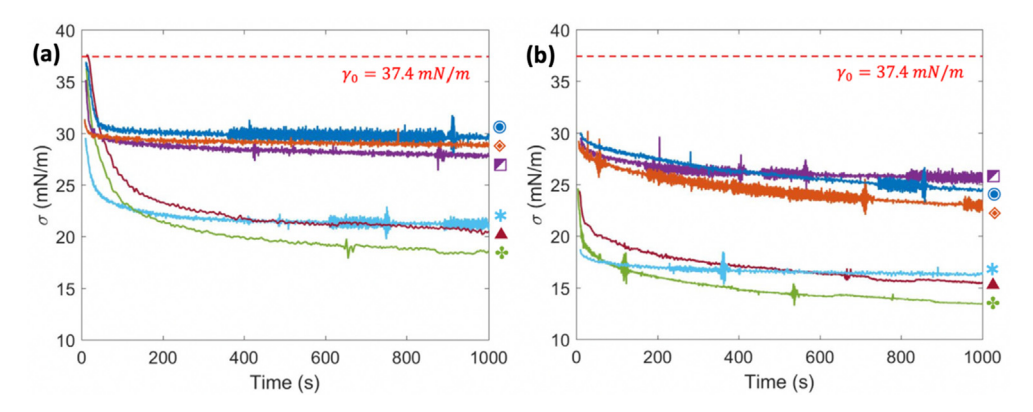


Fig. 2. Dynamic interfacial stress for adsorption from (a) 0.005 wt% or (b) 0.1 wt% polymer xylene solutions (a) H17-B365, H06-B315, H07-B270-SA, H16-B001, H18-B150, H18-B150, H20-B075). The dashed line indicates the interfacial tension of the clean xylene/water interface. Plots that appear to start at lower interfacial tension simply indicate that the initial adsorption rate was too fast to capture the clean interface tension. Data shown are representative of at least 3 replicates for each copolymer.

The current bottlebrush copolymers are xylene-soluble but poorly soluble in water. PEO arm attraction to the aqueous phase would tend to drive adsorption to the interface while the backbone and PBA arms would favor the xylene phase. Nevertheless, the relative abundance of PEO in the copolymers did not uniquely determine the interfacial stress reduction in Fig. 2: H06-B315 and H17-B365 yielded similar long-time interfacial stress reduction. The data in Fig. 2 did not reveal any role of arm length in the interfacial stress reduction: H06-B315 and H07-B270-SA yielded similar longtime stress reduction. Thus, within this data set, no clear interfacial stress reduction trend emerged for the key copolymer composition variables. Despite the lack of a definitive effect of PEO content and arm length on the magnitude of the interfacial stress reduction, both of these characteristics will emerge below as important determinants of the interfacial rheological behaviors and emulsifying efficiency.

#### 3.3. Interfacial dilatational rheology

When the interfacial area is perturbed, there are several possible ways the molecules on the interface, as well as those in the bulk fluid, could relax in response to the perturbation. Interpreting  $\Pi$  – A response curves in terms of dominant relaxation modes is a goal of interfacial rheology. Depending on whether the relaxation process involves exchange of matter with the surrounding bulk fluids or is strictly confined to the interface, "external" or "internal" relaxation modes can be defined. External modes refer to the exchange of molecules from the interface to one or both bulk fluids (desorption) or from a bulk fluid to the interface (adsorption). In contrast, internal modes are those only happening within the interfacial layer and involve the re-organization of species within the adsorbed layer or reconfigurations of the conformation of the adsorbed molecules. Of course, only reconfigurations that detectably influence the interfacial stress are experimentally accessible. Complex macromolecules can exhibit a richer variety of relaxation modes than simple surfactants. Conformational reconfigurations may change the distribution of polymer segments within the finite thickness region of varying composition that defines the interface, or they may change the magnitude of intermolecular repulsions or attractions among segments of the same chain or neighboring

During compression, the interface becomes increasingly crowded and the interfacial pressure would tend to increase. In this situation, the relevant relaxation modes that would counteract the increase of interfacial pressure are desorption and polymer reconfigurations that detach some fraction of polymer segments from the interface and shift more segments toward the bulk. Dur-

ing an expansion process when the interface becomes less crowded, the naturally relevant relaxation modes become adsorption and reconfigurations that shift some polymer segments back to the interface.

3.3.1.  $\Pi$  – A response curves during large-amplitude strain cycling Fig. 3 reports the  $\Pi - A$  response curves for all the copolymer layers as they experienced large-amplitude compression and expansion cycles. For general discussion, we classify those  $\Pi - A$ response curves into four main categories depending on their qualitative shapes. The classifications are based on the slope of the response and whether the compression/expansion loop is closed (non-hysteretic) or open (hysteretic). A corresponding nomenclature is presented along with the data. The data are interpreted in the next two sub-sections in terms of how the molecular structure and the bulk concentration affect the  $\Pi - A$  response. Data will show that the length of the PEO arms and the overall PEO content of the bottlebrush copolymers dictate the form of the response curves, and that a 20-fold increase in bulk concentration subtly alters the hysteretic character of the response curves but with little effect on their curvature.

#### 3.4. Role of molecular structure

Since all the copolymers in this work are insoluble in water, the hydrophilic PEO arms would function as the anchoring groups that fix the polymers at the interface. As a result, increasing the length or overall amount of PEO arms may be anticipated to more tightly anchor the copolymers and therefore disfavor relaxation modes triggered by compression. Whereas trends in interfacial stress reduction with respect to copolymer structure characteristics were difficult to discern in the dynamic interfacial stress in Fig. 2, backbone length, arm length and overall PEO content clearly influenced the general form of the  $\Pi-A$  response curves.

The first comparison will be among copolymers with different backbone lengths but similar PEO content (H16-B001, H20-B075, H18-B150, and H17-B365). The linear diblock copolymer (H16-B001) exhibited a flat (F)  $\Pi$  – A response with small but detectable hysteresis for 0.005 wt% in Fig. 3a-1 (FH+ behavior) and no detectable hysteresis for 0.1 wt% in Fig. 3a-2 (FH– behavior). An FH– behavior indicated that all relaxation modes were able to relax completely during interfacial perturbation. Note that if an infinitely slow perturbation rate were used for interfaces composed of bulk-soluble molecules, every  $\Pi$  – A response curve would be in this FH– category as the molecules must desorb and re-adsorb to the equilibrium established by their equilibrium adsorption isotherm and interfacial equation of state. In the 0.005 wt% solution

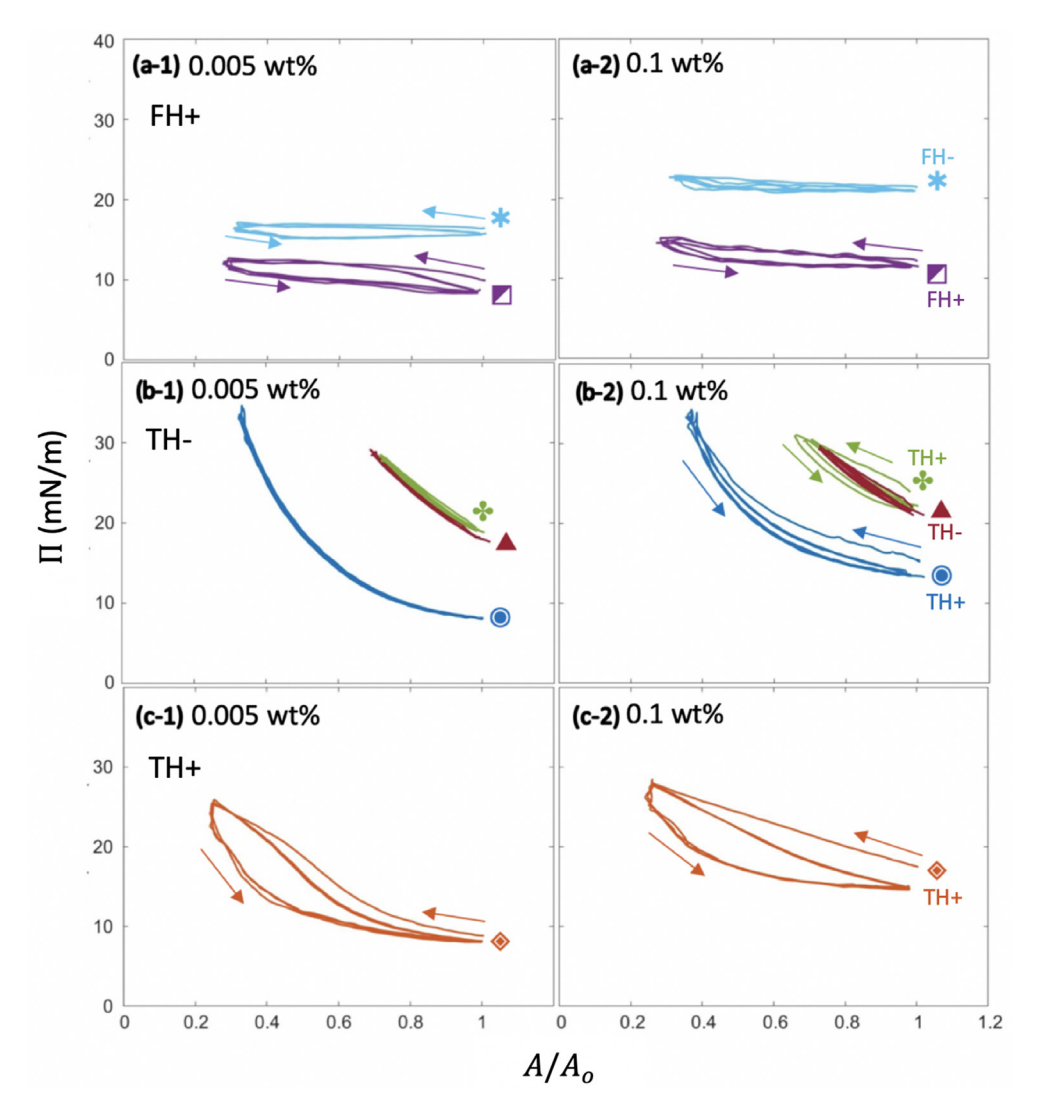


Fig. 3. Π – A response curves during large-amplitude compression and expansion cycles for adsorbed copolymer layers (a) ★ H16-B001, ▼ H07-B270-SA; (b) ♣ H20-B075, ▲ H18-B150, ⑥ H17-B365 and (c) ◈ H06-B315. Interfaces were formed by 1000 s of spontaneous adsorption from 0.005 wt% (left column panels with suffix 1) or 0.1 wt% (right column panels with suffix 2) polymer solutions in xylene. Arrows show the compression or expansion paths in response curves that have a hysteresis loop. Four categories of behaviors (FH-, FH+, TH-, TH+) are defined based on the slope of the curves and the openness of the loops: Flat (F) vs Tilted (T); Non-hysteretic (H-) vs Hysteretic (H+).

experiments, on compression, all modes relaxed completely; while on expansion, the slight hysteresis indicated the modes triggered by expansion were not completely relaxed.

While the linear diblock copolymer H16-B001 exhibited a flat compression response, each of the bottlebrush copolymers with similarly high PEO content (H20-B075, H18-B150 and H17-B365, in Fig. 3 panels b-1 and b-2) exhibited tilted (T) response curves with either small (TH+ behavior) or undetectable (TH- behavior) hysteresis. The tilted character of the response curves indicated that modes triggered by compression were not fully relaxed. In the 0.005 wt% experiments (Fig. 3b-1), none of these high PEO content copolymers exhibited hysteresis. One may therefore conclude that the modes triggered by compression did not undergo further relaxation during the subsequent expansion and that all modes triggered by expansion were fully relaxed during expansion. So, the  $\Pi - A$  response curves traced the same path during the compression and expansion cycles. Hysteresis was observed at higher bulk concentration (Fig. 3b-2). The first compression at 0.1 wt% deviated significantly from the expansion, while all subsequent compression and expansion cycles were only slightly hysteretic (H20-B075 and H17-B365) or else they showed no detectable hysteresis (H18-B150). Thus, except for an interfacial conditioning of some kind that occurred during the first compression, the modes triggered by expansion were "nearly fully" relaxed during all subsequent expansions.

When comparing bottlebrush copolymers with differing PEO content but each having long backbones (H17-B365, in Fig. 3b-1 and 3b2, and H06-B315 in Fig. 3c-1 and 3c-2), both exhibited tilted response curves, indicating incomplete relaxation during compression. The larger PEO content copolymer H17-B365 (TH-) was far less hysteretic than H06-B315 (TH+), indicating that modes were fully relaxed during expansion of interfaces with adsorbed H17-B365 but not so for the low PEO content H06-B315.

The next comparison concerned the effect of arm length for bottlebrush copolymers that otherwise have similar PEO content and a large backbone length (H06-B315 and H07-B270-SA). The shortarm copolymer (H07-B270-SA, Fig. 3a-1 and 3a-2) exhibited the FH+ character with a flat response curve having small but detectable hysteresis: all modes were fully relaxed during compression and nearly fully relaxed upon subsequent expansion. In contrast, the longer-arm copolymer (H06-B315, Fig. 3c-1 and 3c-2) exhibited TH+ behavior with pronounced hysteresis: modes were not fully relaxed during both the compression and the subsequent expansion.

The main effects of copolymer structure shown in Fig. 3 were consistent with the anchoring role of PEO, where the anchoring PEO segments hinders not only a possible complete desorption of copolymers but also any relaxations involving segment detachment from the interface. First, bottlebrush copolymers with longer PEO arms were more prone to incompletely relaxed interfacial modes (tilted response curves) than the short PEO arm bottlebrush (flat response curve). Secondly, with the exception of the shortarm bottlebrush copolymer, bottlebrush copolymers were more prone to incompletely relaxed interfacial modes than the linear diblock copolymer. With a high local density of sidechains, the bottlebrush copolymers would simultaneously present many PEO arms to the interface. Relaxations that would require collective motions of many PEO arms were evidently more hindered than those involving only the single PEO block of the diblock copolymer.

#### 3.5. Role of bulk concentration

In principle, a higher bulk concentration may have at least two effects on the  $\Pi$  – A curves. First, higher bulk concentration would increase the rate of the adsorption relaxation mode during expansion, regardless of whether adsorption was transport-limited or surface-limited. As a consequence, faster adsorption favored by a higher concentration would tend to close the hysteresis loop. This may explain the results for the linear block copolymer H16-B001, where the response curves in Fig. 3a shifted from FH+ to FH- when the bulk concentration was increased from 0.005 wt% (Fig. 3a-1) to 0.1 wt% (Fig. 3a-2). Similarly, a small but observable decrease in the degree of hysteresis occurred with increasing bulk concentration for H07-B270-SA in Fig. 3a. Nevertheless, increasing bulk concentration did not always tend to close the hysteresis loop, and in some cases noted below, increasing concentration increased hysteresis. Relaxation modes other than re-adsorption may also be sensitive to bulk concentration.

The second effect to be noted is that a higher bulk concentration may potentially drive the interface into a different initial state during the formation of the interfacial layers. Macromolecule adsorption entails several competing rate processes. As macromolecules diffuse and adsorb to the interface, their conformation begins to relax toward a more laterally spread state at a rate and to an extent that depends on the coverage of the interface [33,34]. Faster adsorption rates, associated with higher bulk concentrations, may produce adsorbed layers in persistent non-equilibrium states containing more chains in less relaxed conformations that have fewer segments in contact with the interface. Those chains may be more weakly adsorbed.

In the systems under investigation here, this phenomenon could produce a layer where more copolymer molecules were adsorbed from the more concentrated solution, but with a higher fraction of individual copolymers residing in conformations that had a low fraction of PEO segments penetrating the interface. With fewer anchoring segments, the desorption mode (or any mode involving detachment of multiple PEO arms from the interface) might be enhanced during compression. For systems such as H16-B001 and H07-B270-SA (Fig. 3a-1 and a-2) where the desorption mode was already fully relaxed during compression in the low concentration case, increasing concentration had only a modest effect. In contrast, for H20-B075, H17-B365 (Fig. 3b-1 and b-2) and H06-B315 (Fig. 3c-1 and c-2) where modes triggered by compression were not fully relaxed during compression in the low concentration experiments, an enhancement of the desorption (and/or multiple arm detachment) mode favored by fast initial adsorption at high concentration may open the hysteresis loop. This would favor the first compression "conditioning" effect noted for these copolymers in Fig. 3b-2 and for H06-B315 in Fig. 3c-1 and c-2.

#### 3.5.1. $\Pi$ – A response in small-amplitude oscillation cycles

The large-amplitude strain cycling experiments revealed the important role of arm length and PEO content in dictating the form of the  $\Pi - A$  response curves. In contrast, the small-amplitude oscillation data presented in this section will demonstrate that different bottlebrush copolymer structures display quite similar small amplitude behaviors. Fig. 4 shows results of small-amplitude oscillatory dilatation experiments (strain amplitude ~1%) for H20-B075 interfacial layers adsorbed from a 0.005 wt% solution at the highest compression state tested ( $\Pi \sim 26$  mN/m). While quantitative results differed, this behavior was qualitatively representative of all the copolymers considered in this study at multiple interfacial pressures. Fig. 4a shows raw stress and strain data for 1 Hz oscillation, and the same data sampled over ten cycles are plotted as a response curve in Fig. 4b. Apart from the linear diblock copolymer. Fast Fourier Transformation (FFT) of the stress and strain signals (Fig. 4c) revealed only a single peak at the driving frequency, with no higher harmonics that could be distinguished from noise. (The linear diblock produced no FFT signal, either fundamental or higher harmonic, that could be differentiated from noise.) Secondly, for all samples and all conditions, the out-of-phase component of the stress was undetectable (Fig. 4a), leading to the fitted loss modulus falling within experimental error of zero. Thus, the  $\Pi$  – A response curve shown in Fig. 4b exhibited TH- behavior.

The storage and loss components of the complex compression modulus were calculated by fitting data to Eq. [4] (Fig. 4d) for different oscillation frequencies from 0.05 to 1 Hz and plotted in Fig. 4e. Note here that the criterion for calculating a complex compression modulus from the data was that the height of the fundamental peak was at least 5 times greater than the noise background. If not, no modulus was calculated. From 0.05 to 1 Hz, complex moduli were independent of frequency and were dominated by the storage modulus, with negligible contributions from the loss modulus.

The reader is directed to Supporting Information Fig. S9 for the full set of small-amplitude modulus data for all samples and conditions. Bottlebrush copolymers tended to exhibit increasing E' with increasing interfacial pressure, with little difference in the values of E' between the various bottlebrush copolymer structures for a particular interfacial pressure. The only noteworthy difference among the various materials pertained to the value of E' measured at the initial state achieved after 1000 s of adsorption. Samples for which adsorption initially yielded a lower initial interfacial pressure produced a smaller storage modulus at the initial condition. However, when compressing from the initial state, data for all the bottlebrush samples collapsed onto a single master curve of E' vs. II. Of course, the interfacial pressure for the shortarm copolymer H07-B270-SA could not be changed significantly by compressing from its initial state due to its FH+ character, but its initial storage modulus was comparable to the initial moduli produced by other bottlebrush copolymers at a similar initial interfacial pressure.

Since the complex moduli consisted only of the storage modulus and were independent of frequency, the characteristic timescales for any possible relaxation modes were evidently much larger than the timescale of the perturbation up to a frequency of 1 Hz. In the next section, when comparing moduli from large-amplitude strain cycling and small-amplitude strain oscillation, only the storage moduli determined at 1 Hz will be reported to represent results of small-amplitude oscillation experiments.

# 3.5.2. Comparison of moduli from large-amplitude compression and expansion cycles and small-amplitude oscillation

Fig. 5 reports the compression modulus as a function of interfacial pressure from large-amplitude cycling experiments together with the storage modulus determined from small-

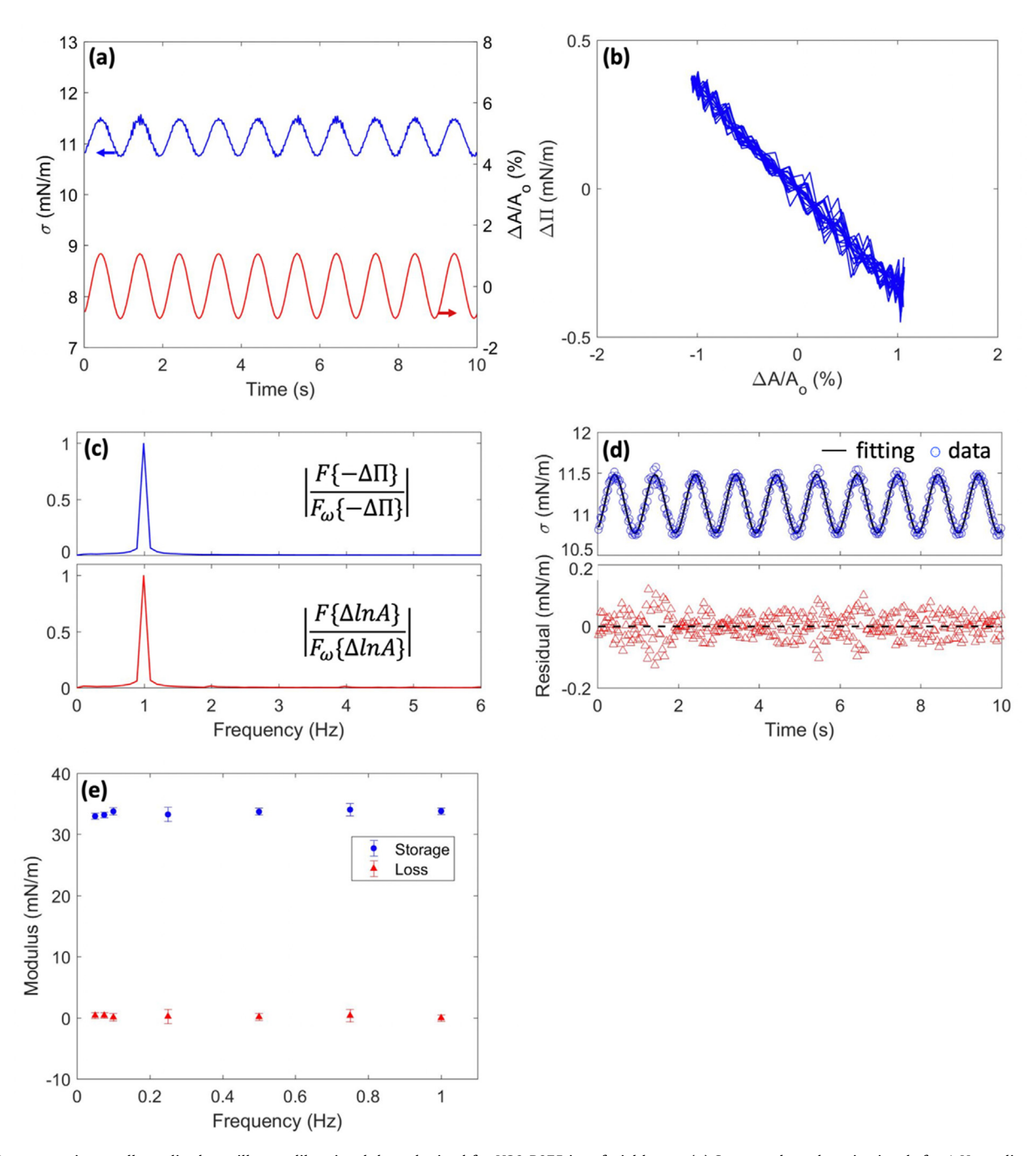


**Fig. 4.** Representative small amplitude oscillatory dilatational data obtained for H20-B075 interfacial layers. (a) Stress and areal strain signals for 1 Hz cycling; (b)  $\Pi$  – A response curve sampled over 10 cycles; (c) magnitudes of FFT for the stress (upper) and the strain (lower) signals normalized by their fundamental frequency signals; (d) fitting of the stress using Eq. [4] (upper) and the residual plot of the fitting (lower); (e) storage and loss modulus as a function of oscillation frequency calculated using Eq. [4]. The error bars represent the 95% confidence interval of the fitted modulus.

amplitude oscillations at varying interfacial pressure for each copolymer. A difference between the two types of moduli for a given interfacial pressure would indicate that the mechanical properties of the adsorbed layers – and therefore the microscopic state of the adsorbed layers – are not uniquely determined by the interfacial pressure but instead depend on the strain history of the interface. Although adsorbed macromolecular layers are prone to persistent non-equilibrium states and may therefore be expected to exhibit history-dependent microscopic states, results presented below indicate that some of the copolymer layers exhibited history-independent mechanical properties. For those systems, interfacial pressure does appear to uniquely specify the microscopic state of the adsorbed layers.

For the linear block copolymer H16-B001 and the short arm bottlebrush copolymer H07-B270-SA (Fig. 5a) the compression modulus could only be probed in a narrow range of interfacial pressures as a result of their FH+ response behavior, with a nearly constant interfacial pressure during compression. Their storage moduli were measured from small amplitude oscillatory experiments only at their initial state. The small amplitude complex modulus was below the detection limit for H16-B001. This distinguished the linear diblock H16-B001, for which all relaxation modes were nearly fully relaxed in the large amplitude cycling experiments (see Fig. 3a), from the bottlebrush copolymers for which one or more relaxation modes failed to relax in the large amplitude experiments, as noted below. Although the diblock

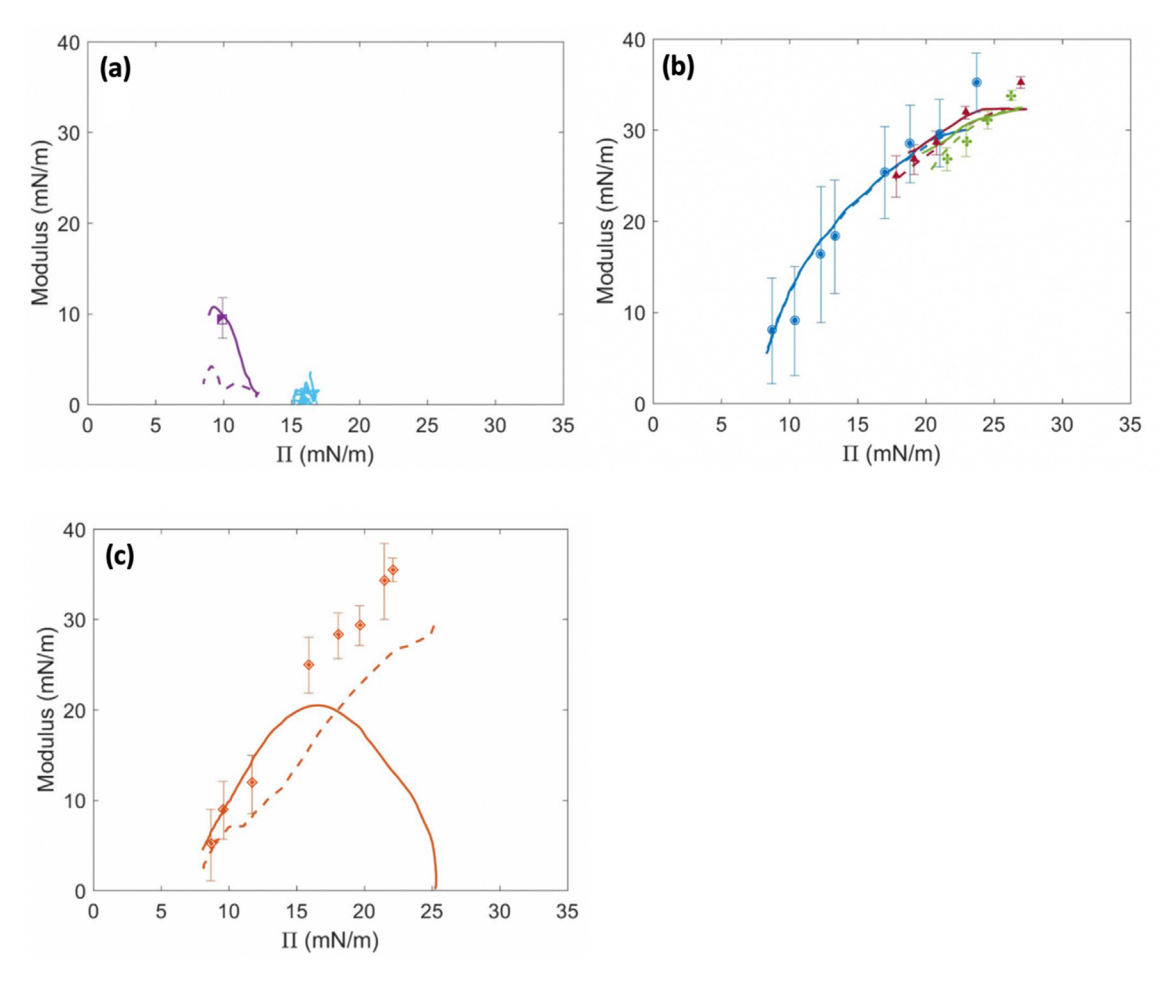


Fig. 5. Interfacial pressure dependence of moduli for copolymers (a) ★ H16-B001, ► H07-B270-SA; (b) ★ H20-B075, ▲ H18-B150, ⑥ H17-B365 and (c) ◈ H06-B315. Curves represent the compression modulus from the third compression (solid curve) and third expansion (broken curve) in the large-amplitude experiments. Data points represent the storage modulus measured at 1 Hz in small-amplitude oscillation experiments at the indicated interfacial pressure. Error bars are 95% confidence intervals for the fitted modulus from Eq. [4]. The interfacial layers were formed by spontaneous adsorption from 0.005 wt% solutions.

copolymer produced the greatest interfacial stress reduction by spontaneous adsorption, the fact that it produced negligibly small compression or storage moduli shows that it provided nearly no resistance to interfacial dilatation: its relaxations were faster than any of the imposed strain perturbations.

For copolymers H20-B075, H18-B150 and H17-B365 (Fig. 5b) that have similar PEO content but varying backbone lengths, the compression modulus increased monotonically with increasing interfacial pressure, and the storage modulus from small amplitude oscillation experiments closely matched the large-amplitude compression modulus across the full range of interfacial pressures. Most notably, for these materials, their modulus vs. interfacial pressure curves overlapped to create a single curve in Fig. 5b, with minimal difference between moduli achieved during compression or during expansion and no significant difference between large and small amplitude strain measurements. Thus, the interfacial pressure appeared to uniquely determine the microscopic state of the adsorbed layers, with no dependence on strain history on timescales ranging from 1 s to ~30 min.

For the low PEO content bottlebrush copolymer H06-B315 (Fig. 5c), the large amplitude compression modulus passed through a maximum when increasing interfacial pressure (compression indicated by the solid curve in Fig. 5c) but dropped monotonically when subsequently decreasing the interfacial pressure (expansion indicated by the dashed curve). The discrepancy between the compression and expansion curves corresponded to the open hystere-

sis loop for the TH+ response curve behavior (Fig. 3c-1). The storage modulus from small amplitude oscillation measurements initially tracked the compression modulus at low interfacial pressures but diverged from the compression modulus at an interfacial pressure of ~15 mN/m, which also corresponded to the location of the maximum in the large amplitude compression modulus measured during the compression stage. Beyond that point, the small amplitude storage modulus continued to increase with increasing interfacial pressure, tracking somewhat above the compression modulus that was measured upon the re-expansion of the interface in the large amplitude measurements.

The large differences between the small amplitude storage modulus and the large amplitude compression modulus at high interfacial pressures indicate changes in the microstructure of the adsorbed H06-B315 layer, leading to some newly activated modes. Although different experimental probes would be needed to verify the nature of the newly activated modes, they might arise from processes such as polymer aggregation or expulsion of chains into local multilayer patches that yield slower reconfigurations. Alternatively, higher amplitude compression may activate increasing amounts of desorption, and the openness of the loop may be simply a consequence of slow re-adsorption and reconfiguration during expansion.

To summarize, the pendant drop tensiometry and interfacial rheology measurements demonstrated that although no definitive relationships were discernible between bottlebrush copolymer structural characteristics and the degree of interfacial stress reduction produced by spontaneous adsorption, there were distinct relationships between structural characteristics and the interfacial dilatational rheological behaviors. The differences among different bottlebrush structures were more pronounced in the large-amplitude strain cycling than in small-amplitude strain oscillation measurements. The final section seeks a correlation with emulsifying efficiency.

#### 3.6. Emulsifying efficiency

Emulsification tests were conducted to determine the lowest copolymer concentration capable of forming a stable water-in-oil emulsion. An emulsifier that produces a stable emulsion at the lowest concentration is considered the one with the highest emulsifying efficiency. Since these polymers belong to the class of "nanoscale brushes" that enable emulsions with long shelf-lives at low concentrations with no other additives, a rather stringent criterion was adopted whereby an emulsion was judged to be stable only if there was no detectable growth in the neat aqueous phase volume for at least one month after preparation. Stability here did not refer to resistance against sedimentation. Apart from the short-arm bottlebrush copolymer, all of the copolymers were capable of producing a stable emulsion using 0.1 wt% concentrations or less, and all resulting emulsions were determined to be water-in-xylene by the drop test. In all cases, 100% of the aqueous phase was emulsified: no neat aqueous phase existed after the initial homogenization. The droplet sizes had a rather broad distribution, ranging from tens to hundreds of micrometers for all bottlebrush copolymers, while the distribution was narrower (around tens of micrometers) for the linear diblock copolymer [30].

Table 2 reports the emulsifying efficiency determined for each sample along with their interfacial characteristics which may correlate with the efficiency. All interfacial measurements were made on layers formed by spontaneous adsorption from 0.005 wt% solutions in xylene. When the emulsifying efficiency is reported in the table as <0.0025 wt%, it indicates that a stable emulsion was produced at 0.0025 wt%, which was the lowest concentration tested. In the following, each interfacial characteristic was examined to determine which is most closely associated with emulsifying efficiency. The discussion focuses on the bottlebrush copolymers, followed by comments on the diblock copolymer.

#### 3.7. Role of interfacial stress reduction at initial state: $\sigma_{initial}$

When discerning trends among the bottlebrush copolymers, the reduction in the interfacial stress at the initial state,  $\sigma_{\rm initial}$ , is not sufficient to distinguish the emulsifying efficiency. The three high PEO content copolymers, H17-B365, H20-B075 and H18-B150, all exhibited the highest emulsifying efficiency, but the one with longest backbone (H17-B365) produced significantly less interfacial

stress reduction by adsorption from solution. Also, H17-B365 produced a similar interfacial stress reduction as the lower PEO content copolymers H06-B315 and H07-B270-SA, but they showed extremely different emulsifying efficiencies.

# 3.8. Role of small amplitude oscillatory storage modulus at initial state: $E_{initial}^{\prime}$

The next feature examined is the value of the small amplitude oscillatory storage modulus measured at the initial state achieved by spontaneous adsorption from solution,  $E'_{initial}$ . Again, this feature did not serve to identify the most efficient emulsifiers. This was evident when comparing the high PEO content H17-B365 and the low PEO content H06-B315 and the short-arm sample H07-B270-SA. These had comparable storage moduli at their initial states but the more hydrophilic bottlebrush H17-B365 showed significantly higher emulsifying efficiency. Also, H17-B365 had a much smaller  $E'_{initial}$  than either H18-B150 or H20-B075, yet these three materials all had the same high emulsifying efficiency.

# 3.9. Role of the attainable magnitude of the small amplitude oscillatory storage modulus

While the initial storage modulus failed to distinguish copolymers according to their emulsifying efficiency, it was next considered whether the ability to attain a large storage modulus when conducting small-amplitude oscillatory rheology measurements on compressed layers at high interfacial pressure may do so. The trends reported in Fig. 5 show that this characteristic also fails. While H06-B315 was a significantly less efficient emulsifier than H20-B075, H18-B150 and H17-B365, it exhibited small-amplitude oscillatory storage moduli that were very similar to those generated by H20-B075, H18-B150 and H17-B365 across a range of interfacial pressures (compare small-amplitude data in Fig. 5b and c).

#### 3.10. Role of the $\Pi$ – A response curve category

Finally, the key interfacial characteristic that was able to distinguish bottlebrush copolymers according to their emulsifying efficiency was found to be the form of the  $\Pi$  – A response curve determined in large-amplitude strain cycling experiments. The bottlebrush copolymers producing TH— behavior (H20-B075, H18-B150, H17-B365) were significantly more efficient emulsifiers than all the other bottlebrush copolymers. The next most efficient bottlebrush emulsifier was the less hydrophilic H06-B315 which showed TH+ behavior, and the least efficient emulsifier was the short arm H07-B270-SA which showed FH+ behavior. Higher emulsifying efficiency was associated with adsorbed layers that generated increasingly large compression moduli with increasing interfacial pressure. The distinction between the most efficient

**Table 2**Comparison among different copolymer structural and rheological characteristics and emulsifying efficiency

Copolymer	Molecular Variable comparisons	$\sigma_{initial}^{\;a}$ [mN/m]	E <sub>initial</sub> <sup>b</sup> [mN/m]	$\Pi - A$ curve category <sup>c</sup>	Emulsifying efficiency <sup>d</sup>	
H16-B001	Backbone length		22	B.D.	FH+	0.005-0.01 wt% [30]
H20-B075			18	27	TH-	<0.0025 wt%
H18-B150			20	25	TH-	<0.0025 wt%
H17-B365	PEO wt%		30	8	TH-	<0.0025 wt% [30]
H06-B315		Arm length	29	5	TH+	0.01-0.02 wt% [30]
H07-B270-SA			28	10	FH+	>0.1 wt% [30]

a Interfacial stress measured at the initial state. The uncertainty was at most 2 mN/m based on at least 3 replicate measurements for each sample.

<sup>&</sup>lt;sup>b</sup> Storage moduli measured at the initial state from small-strain oscillation experiments. B.D. means "below detectability". The uncertainty was less than 5 mN/m based on the 95% confidence interval from the least-squares fitting. (See Supporting Information Fig. S9.)

 $<sup>^{\</sup>rm c}$   $\Pi$  – A curve category is based on the large-strain cycling experiments.

<sup>&</sup>lt;sup>d</sup> Concentrations tested: 0.0025, 0.005, 0.01, 0.02, 0.05, and 0.1 wt%.

emulsifiers (H20-B075, H18-B150, and H17-B365) and the next most efficient emulsifier (H06-B315) was that H06-B315 exhibited a threshold interfacial pressure of ~15 mN/m above which the compression modulus measured in large-amplitude strain experiments passed through a maximum and approached zero as the interfacial pressure reached 25 mN/m. The adsorbed layer thereby presented less resistance to compression at higher interfacial pressures, effectively a "softening" of the interface at high compression, which was not evident in the small amplitude oscillatory storage modulus data. Similar occurrences of adsorbed layer softening at high compression have been observed previously for monolayers of pulmonary surfactants [31], some amphiphilic block copolymers [35] and cellulose nanocrystals [36].

In contrast, the large-amplitude compression moduli of the three most efficient bottlebrush emulsifiers continued to increase up to the highest interfacial pressures sampled, with moduli exceeding 30 mN/m and still increasing as the interfacial pressure reached 25 mN/m. The adsorbed layers for the three most efficient emulsifiers effectively "stiffened" at high compression. It is possible that these layers would also pass through a maximum compression modulus at even higher interfacial pressures, but these were not accessible due to drop detachment from the needle at the critical Bond number attained at interfacial pressures slightly above the range tested here.

Previously, adsorbed layers of multi-arm PEO star polymers at the oil/water interface were found to exhibit this trend of increasing compression modulus with increasing interfacial pressure and to be far more efficient emulsifiers than linear PEO homopolymers which provided similar interfacial tension reduction by adsorption but only a negligible compression modulus [3]. The present work further establishes that among materials that exhibit the trend of increasing modulus with increasing interfacial pressure, the characteristic of a threshold softening interfacial pressure during large amplitude compression can be the main distinguishing interfacial rheological characteristic. The most efficient bottlebrush emulsifiers did *not* exhibit the softening behavior.

The concept of emulsifying efficiency involves processes occurring not only during the initial homogenization but also during prolonged emulsion storage. It entails interfacial dynamics over a wide range of time scales and strain amplitudes. The current study examines widely varying strain amplitudes, but the highest emulsification-relevant frequencies are not accessible by the techniques used here. It is nevertheless compelling that bottlebrush copolymer structural differences are correlated with distinctive characteristics of the large-amplitude  $\Pi$  – A response curves and also that the most efficient bottlebrush copolymer emulsifiers share the same type of  $\Pi$  – A response curve that exhibits a monotonically increasing compressional modulus with increasing interfacial pressure. A direct empirical connection is drawn from the bottlebrush molecular structure to the large-amplitude  $\Pi - A$ response curve category, and from there to the emulsifying efficiency. Meanwhile, no correlation could be found between the small-amplitude storage modulus behaviors and either the emulsifying efficiency or the bottlebrush copolymer structural characteristics. The results presented here should motivate future research to determine how the response of bottlebrush copolymers to large amplitude strains becomes an important aspect of the mechanisms responsible for efficient emulsification.

### 3.11. The outsider: linear diblock copolymer

The linear diblock copolymer H16-B001 exhibited FH+ behavior with little resistance to dilatation. It had small compression and storage moduli, yet its emulsifying efficiency was superior to that of the bottlebrush copolymer H06-B315, which exhibited TH+ behavior and larger moduli. Between those two polymers, the

diblock copolymer produced significantly greater interfacial stress reduction by spontaneous adsorption (Fig. 2), but its dilatational rheology behaviors would have placed it in a grouping with the least efficient bottlebrush emulsifiers. Given that many factors play a role in emulsification, the cautious interpretation is that interfacial rheology trends only correlate with emulsifying efficiency within the same class of material, such as the nanoscale brushes considered here.

#### 4. Conclusions

A series of amphiphilic, xylene-soluble heterografted PEO-PBA bottlebrush copolymers with varying backbone length, hydrophilicity (PEO content) and arm length were synthesized via ATRP for interfacial dilatational rheology analysis at the xylene-water interface and correlation with emulsifying efficiency. These materials are of interest as high efficiency emulsifiers, and it was hypothesized that bottlebrush structural differences would yield differences in dilatational rheological characteristics that correlate with differences in emulsifying efficiency.

Interfacial rheology results reveal molecular structure characteristics that favor larger compression and storage moduli in adsorbed layers. The length of the arms is a key molecular parameter. Whereas copolymers with shorter arms produce layers that increase only modestly in interfacial pressure in response to large amplitude compression, those with longer arms can be compressed to large interfacial pressures at which they exhibit significantly larger compressional and storage moduli. Overall PEO content is also important. Comparing bottlebrush copolymers with different PEO content but similar arm length, greater PEO content eliminates hysteresis in the  $\Pi$  – A response curve. These observations are consistent with the role of PEO to anchor the copolymers to the xylene/water interface and thereby to hinder the relaxations that involve segment detachment from the interface. Comparison of moduli obtained from large-amplitude strain cycling and smallamplitude strain oscillation measurements reveal that interfacial pressure uniquely fixes the microscopic state of adsorbed bottlebrush copolymers that have a sufficient PEO content; decreased PEO content or arm length yields microscopic states that depend on strain history.

Although a larger copolymer test library would be helpful, a correlation begins to emerge between interfacial dilatational rheology characteristics and emulsifying efficiency. Our prior work indicated a favorable correlation between the existence of a large dilatational modulus and the ability to produce a stable emulsion when comparing PEO polymers with different architectures (homopolymer vs. multi-arm star polymer) [3]. The current study further indicates that the existence of a significant dilatational modulus alone does not adequately distinguish between the most efficient and less efficient emulsifiers. The efficiency can differ significantly even for systems that exhibit similar compression or storage moduli at their initial adsorption state or even at higher compression states. The most efficient bottlebrush emulsifiers are those that exhibit interfacial stiffening behavior such that the large-amplitude compressional modulus increases monotonically with increasing interfacial pressure. The less efficient bottlebrush emulsifiers are those that soften, or display a decreasing modulus with increasing compression beyond a threshold interfacial pressure.

For comparison purposes, the moduli measured here are similar in magnitude, up to ~30 mN/m, to those of adsorbed layers formed by adsorption of multi-arm PEO star polymers [3] and cationic polyelectrolyte-grafted silica nanoparticles [21]. However, these moduli are significantly smaller than those that have been reported for some dense layers of insoluble surfactants [37], lipids

[38], nanoparticles [39] or gel-forming proteins [40], for which moduli can exceed 100 mN/m. This work is, to our knowledge, the first report on the interfacial rheology of bottlebrush copolymers, which deepens the fundamental understanding of basic interfacial phenomena for an emerging class of surface-active materials.

Future work should expand the bottlebrush copolymer sample set to more precisely identify the PEO content boundary that marks the transition from softening to stiffening interfacial rheological behavior and further test the correlation with emulsifying efficiency. Within this bottlebrush series, direct probes of adsorbed layer configurations and interfacial excess concentrations would provide important insights into the origins of hysteretic response curves or strain-history dependent microscopic states for the low PEO content bottlebrush. Finally, new bottlebrush chemistries should be investigated to determine whether the correlation between interfacial stiffening behavior and more efficient emulsification holds for other systems as well.

#### **Declaration of Competing Interest**

The authors declare that they have no known competing financial interests or personal relationships that could have appeared to influence the work reported in this paper.

#### Acknowledgment

This material is based on work supported by the National Science Foundation under grant CBET-1705432 and DMR 1501324.

#### Appendix A. Supplementary data

Supplementary data to this article can be found online at https://doi.org/10.1016/j.jcis.2020.07.063.

### References

- [1] K.A. Erk, J.D. Martin, J.T. Schwalbe, F.R. Phelan, S.D. Hudson, Shear and dilational interfacial rheology of surfactant-stabilized droplets, J. Colloid Interface Sci. 377 (2012) 442–449, https://doi.org/10.1016/j.jcis.2012.03.078.
- [2] D. Langevin, F. Monroy, Interfacial rheology of polyelectrolytes and polymer monolayers at the air-water interface, Curr. Opin. Colloid Interface Sci. 15 (2010) 283–293, https://doi.org/10.1016/j.cocis.2010.02.002.
- [3] Y.-R. Huang, M. Lamson, K. Matyjaszewski, R.D. Tilton, Enhanced interfacial activity of multi-arm poly(ethylene oxide) star polymers relative to linear poly (ethylene oxide) at fluid interfaces, Phys. Chem. Chem. Phys. 19 (2017) 23854–23868, https://doi.org/10.1039/C7CP02841E.
- [4] E.M. Freer, K.S. Yim, G.G. Fuller, C.J. Radke, Interfacial rheology of globular and flexible proteins at the hexadecane/water interface: comparison of shear and dilatation deformation, J. Phys. Chem. B. 108 (2004) 3835–3844, https://doi. org/10.1021/jp037236k.
- [5] F.S. Ariola, A. Krishnan, E.A. Vogler, Interfacial rheology of blood proteins adsorbed to the aqueous-buffer/air interface, Biomaterials 27 (2006) 3404– 3412, https://doi.org/10.1016/j.biomaterials.2006.02.005.
- [6] J.H.J. Thijssen, J. Vermant, Interfacial rheology of model particles at liquid interfaces and its relation to (bicontinuous) Pickering emulsions, J. Phys. Condens. Matter. 30 (2018), https://doi.org/10.1088/1361-648X/aa9c74.
- [7] A.J. Mendoza, E. Guzmán, F. Martínez-Pedrero, H. Ritacco, R.G. Rubio, F. Ortega, V.M. Starov, R. Miller, Particle laden fluid interfaces: dynamics and interfacial rheology, Adv. Colloid Interface Sci. 206 (2014) 303–319, https://doi.org/ 10.1016/j.cis.2013.10.010.
- [8] R. Van Hooghten, V.E. Blair, A. Vananroye, A.B. Schofield, J. Vermant, J.H.J. Thijssen, Interfacial rheology of sterically stabilized colloids at liquid interfaces and its effect on the stability of pickering emulsions, Langmuir 33 (2017) 4107–4118, https://doi.org/10.1021/acs.langmuir.6b04365.
- [9] C. Dicharry, D. Arla, A. Sinquin, A. Graciaa, P. Bouriat, Stability of water/crude oil emulsions based on interfacial dilatational rheology, J. Colloid Interface Sci. 297 (2006) 785–791, https://doi.org/10.1016/j.jcis.2005.10.069.
- [10] D. Georgieva, V. Schmitt, F. Leal-Calderon, D. Langevin, On the possible role of surface elasticity in emulsion stability, Langmuir 25 (2009) 5565–5573, https://doi.org/10.1021/la804240e.
- [11] A. Stocco, W. Drenckhan, E. Rio, D. Langevin, B.P. Binks, Particle-stabilised foams: an interfacial study, Soft Matter 5 (2009) 2215–2222, https://doi.org/ 10.1039/b901180c.

- [12] A. Cervantes Martinez, E. Rio, G. Delon, A. Saint-Jalmes, D. Langevin, B.P. Binks, On the origin of the remarkable stability of aqueous foams stabilised by nanoparticles: link with microscopic surface properties, Soft Matter 4 (7) (2008) 1531, https://doi.org/10.1039/b804177f.
- [13] J. Lucassen, M. Van Den Tempel, Dynamic measurements of dilational properties of a liquid interface, Chem. Eng. Sci. 27 (1972) 1283–1291, https://doi.org/10.1016/0009-2509(72)80104-0.
- [14] J. Lucassen, Adsorption kinetics in micellar systems, Faraday Discuss. Chem. Soc. 59 (1975) 76–87, https://doi.org/10.1039/DC9755900076.
- [15] M. van den Tempel, E.H. Lucassen-Reynders, Relaxation processes at fluid interfaces, Adv. Colloid Interface Sci. 18 (1983) 281–301, https://doi.org/ 10.1016/0001-8686(83)87004-3.
- [16] E.V. Aksenenko, V.I. Kovalchuk, V.B. Fainerman, R. Miller, Surface dilational rheology of mixed adsorption layers at liquid interfaces, Adv. Colloid Interface Sci. 122 (2006) 57–66, https://doi.org/10.1016/j.cis.2006.06.012.
- [17] B.A. Noskov, Dynamic surface elasticity of polymer solutions, Colloid Polym. Sci. 273 (1995) 263–270, https://doi.org/10.1007/BF00657833.
- [18] B.A. Noskov, Protein conformational transitions at the liquid gas interface as studied by dilational surface rheology, Adv. Colloid Interface Sci. 206 (2014) 222–238, https://doi.org/10.1016/j.cis.2013.10.024.
- [19] B.A. Noskov, A.A. Mikhailovskaya, S. Lin, G. Loglio, R. Miller, Bovine serum albumin unfolding at the air/water interface as studied by dilational surface, Rheology 26 (2010) 17225–17231, https://doi.org/10.1021/la103360h.
- [20] B.A. Noskov, A.V. Latnikova, S. Lin, G. Loglio, R. Miller, Dynamic surface elasticity of -casein solutions during, Adsorption (2007) 16895–16901, https://doi.org/10.1021/jp073813j.
- [21] N.J. Alvarez, S.L. Anna, T. Saigal, R.D. Tilton, L.M. Walker, Interfacial dynamics and rheology of polymer-grafted nanoparticles at air-water and xylene-water interfaces, Langmuir 28 (2012) 8052–8063, https://doi.org/10.1021/ la300737p.
- [22] E. Santini, L. Liggieri, L. Sacca, D. Clausse, F. Ravera, Interfacial rheology of Span 80 adsorbed layers at paraffin oil – water interface and correlation with the corresponding emulsion properties, Colloids Surfaces A: Physicochem. Eng. Aspects 309 (2007) 270–279, https://doi.org/10.1016/j.colsurfa.2006.11.041.
- [23] N. Aske, R. Orr, J. Sjöblom, Dilatational elasticity moduli of water crude oil interfaces using the oscillating pendant drop dilatational elasticity moduli of water – crude oil interfaces using the oscillating pendant drop, J. Dispers. Sci. Technol. 2691 (2007), https://doi.org/10.1081/DIS-120015978.
- [24] X. Yang, V.J. Verruto, P.K. Kilpatrick, N. Carolina, R.V. September, V. Re, M. Recei, V. December, A.B. Th, Dynamic asphaltene resin exchange at the oil/ water interface: time-dependent W/O emulsion stability for asphaltene/resin model oils, Energy Fuels 64 (2007) 1343–1349, https://doi.org/10.1021/ef060465w.
- [25] T. Saigal, H. Dong, K. Matyjaszewski, R.D. Tilton, Pickering emulsions stabilized by nanoparticles with thermally responsive grafted polymer brushes, Langmuir 26 (2010) 15200–15209, https://doi.org/10.1021/la1027898.
- [26] T. Saigal, A. Yoshikawa, D. Kloss, M. Kato, P.L. Golas, K. Matyjaszewski, R. D. Tilton, Stable emulsions with thermally responsive microstructure and rheology using poly(ethylene oxide) star polymers as emulsifiers, J. Colloid Interface Sci. 394 (2013) 284–292, https://doi.org/10.1016/j.jcis.2012.11.033.
- [27] N. Saleh, T. Sarbu, K. Sirk, G.V. Lowry, K. Matyjaszewski, R.D. Tilton, Oil-in-water emulsions stabilized by highly charged polyelectrolyte-grafted silica nanoparticles, Langmuir 21 (2005) 9873–9878, https://doi.org/10.1021/1a050654r.
- [28] W. Li, Y. Yu, M. Lamson, M.S. Silverstein, R.D. Tilton, K. Matyjaszewski, PEO-based star copolymers as stabilizers for water-in-oil or oil-in-water emulsions, Macromolecules 45 (2012) 9419–9426, https://doi.org/10.1021/ma3016773.
- [29] T. Saigal, J. Xu, K. Matyjaszewski, R.D. Tilton, Emulsification synergism in mixtures of polyelectrolyte brush-grafted nanoparticles and surfactants, J. Colloid Interface Sci. 449 (2015) 152–159, https://doi.org/10.1016/j. icis 2014 12 047
- [30] G. Xie, P. Krys, R.D. Tilton, K. Matyjaszewski, Heterografted molecular brushes as stabilizers for water-in-oil emulsions, Macromolecules 50 (2017) 2942– 2950, https://doi.org/10.1021/acs.macromol.7b00006.
- [31] A.G. Bykov, G. Loglio, R. Miller, O.Y. Milyaeva, A.V. Michailov, B.A. Noskov, Dynamic properties and relaxation processes in surface layer of pulmonary surfactant solutions, Colloids Surfaces A Physicochem. Eng. Asp. 573 (2019) 14–21, https://doi.org/10.1016/j.colsurfa.2019.04.032.
- [32] H. Gao, K. Matyjaszewski, Synthesis of miktoarm star polymers via ATRP using the "in-out" method: Determination of initiation efficiency of star macroinitiators, Macromolecules 39 (2006) 7216–7223, https://doi.org/ 10.1021/ma061702x.
- [33] Y. Tie, C. Calonder, P.R. Van Tassel, Protein adsorption: kinetics and history dependence, J. Colloid Interface Sci. 268 (2003) 1–11, https://doi.org/10.1016/ S0021-9797(03)00516-2.
- [34] H.M. Schneider, P. Frantz, S. Granick, The bimodal energy landscape when polymers adsorb, Langmuir 12 (1996) 994–996, https://doi.org/10.1021/ 13950556d
- [35] A. Moghimikheirabadi, P. Fischer, M. Kröger, L.M.C. Sagis, Relaxation behavior and nonlinear surface rheology of PEO-PPO-PEO triblock copolymers at the airwater interface, Langmuir 35 (2019) 14388–14396, https://doi.org/10.1021/ acs.langmuir.9b02540.
- [36] S. Kuster, E.J. Windhab, L.M.C. Sagis, P. Fischer, Nonlinear shear and dilatational rheology of viscoelastic interfacial layers of cellulose nanocrystals, Phys. Fluids 072103 (2018), https://doi.org/10.1063/1.5035334.

- [37] A.P. Kotula, S.L. Anna, Insoluble layer deposition and dilatational rheology at a microscale spherical cap interface, Soft Matter 12 (2016) 7038–7055, https://doi.org/10.1039/c5sm03133h.
- [38] M. Vrânceanu, K. Winkler, H. Nirschl, G. Leneweit, Surface rheology of monolayers of phospholipids and cholesterol measured with axisymmetric drop shape analysis, Colloids Surfaces A Physicochem. Eng. Asp. 311 (2007) 140–153, https://doi.org/10.1016/j.colsurfa.2007.06.008.
- [39] S.M. Kirby, S.L. Anna, L.M. Walker, Effect of surfactant tail length and ionic strength on the interfacial properties of nanoparticle-surfactant complexes, Soft Matter 14 (2017) 112–123, https://doi.org/10.1039/c7sm01806a.
- [40] J.T. Petkov, T.D. Gurkov, B.E. Campbell, R.P. Borwankar, Dilatational and shear elasticity of gel-like protein layers on air/water interface, Langmuir 16 (2000) 3703–3711, https://doi.org/10.1021/la991287k.